Materials Chemistry and Physics 120 (2010) 319–322

Contents lists available at ScienceDirect

Materials Chemistry and Physics

journal homepage: www.elsevier.com/locate/matchemphys

Electron irradiation effect and photoluminescence properties of ZnO-tetrapod nanostructures

Mashkoor Ahmad [a], Caofeng Pan [a], Jiong Zhao [a], Javed Iqbal [b], Jing Zhu [a,*]

[a] Beijing National Center for Electron Microscopy, The State Key Laboratory of New Ceramics and Fine Processing, Laboratory of Advanced Material, China Iron & Steel Research Institute Group, Department of Material Science and Engineering, Tsinghua University, Beijing 100084, China
[b] Laboratory of Advanced Materials, Department of Material Science and Engineering, Tsinghua University, Beijing 100084, China

ARTICLE INFO

Article history:
Received 24 April 2009
Received in revised form 5 November 2009
Accepted 7 November 2009

Keywords:
ZnO
Nanostructure
Defects
Tunneling
Electron irradiation
Photoluminescence

ABSTRACT

The effect of high-energy (200 keV) electron irradiation on ZnO-tetrapod (ZnO-T) nanostructure has been investigated by employing in situ scanning tunneling microscopy (STM) holder inside TEM. The microscopic results have revealed that the product consists of highly single-crystalline ZnO-T structures. The photoluminescence spectra show the increased amount of defects which lead to shift in the emission peak position in ultraviolet (UV) region and enhance the PL performance in visible luminescence (VL) region of ZnO-T nanocrystals. The in situ measurements show asymmetric Schottky contacts at the both ends interfaces under electron irradiation. The current–voltage (I–V) characteristics have revealed that the increase in electron density (range of ~0–25 pA cm^{-2}) leads to an increase in the current along with the increase in carrier concentration from 1.1×10^{17} cm^{-3} to 3.2×10^{17} cm^{-3}. In addition, it has been interestingly found that at high bias voltage, Schottky contacts turn to Ohmic contacts at the both ends with the influence of irradiation–matter interaction. The results strongly suggest that the ZnO-T is considered as a promising candidate for applications in irradiation environments.

1. Introduction

ZnO is a wide-bandgap semiconductor (E_g = 3.37 eV) with a large exciton binding energy (60 meV) that makes it a leading candidate material for optoelectronics applications. One–dimensional ZnO nanostructures, such as nanowires [1], nanobelts [2] and nanotetrapods [3–6], have attracted great interest because of their novel physical properties and their applications in spintronics, piezoelectric transducers and optoelectronic devices [7]. Among the nanostructure ZnO-tetrapod (ZnO-T) has received considerable attention because of its unique properties such as the ability to grow branch points of different material onto existing tetrapod structures. The excellent electrical properties of ZnO make it useful in high temperature, high power and high speed electronic devices. Studies on the high-energy electron irradiation (HEEI) experiments give important information about the defects affecting the optical and electrical properties of the material. These studies generally show that HEEI produces less severe damage in ZnO than that of GaN and SiC known as more radiation resistant than classical semiconductor such as Si and GaAs [8,9]. Also, rapid defect annihilation of ZnO even at low temperature plays an important role in becoming radiation hard material besides its crystallographic strength [10]. Since most of the solid state devices need metal–semiconductor contacts, it also specifically become important to understand the behavior of metal–semiconductor structure under particle irradiation. In order to investigate the metal–semiconductor contacts behavior piezo-holders are exciting tools that enable electrical measurements inside a TEM [11]. In the literature according to our knowledge, only few groups have been reported the electrical response of ZnO-T under UV illumination [12–14]. However, electrical response of ZnO-T under electron irradiation has not been reported yet. Here in this letter, we are reporting the electrical response of individual ZnO-T via in situ high-resolution transmission electron microscopy technique.

2. Experimental

Syntheses of ZnO-Ts are carried out in a horizontal quartz tube furnace via chemical vapor deposition. In this process a crucible containing the metallic Zn powder is loaded in the central region of the quartz tube furnace. A Si substrate is placed downstream from the crucible as the collector. The quartz tube is heated to 700 °C for 3 h. Ar carrier gas with an O_2 content of 5% are introduced into the tube at a flow rate of 150 sccm. After the reaction is terminated, the products are collected. The as-prepared products are examined by scanning electron microscope (SEM-JEM6301-F), high-resolution transmission electron microscope (HRTEM-JEM-2011). Photoluminescence (PL) measurement is conducted at room temperature using the 325 nm line of a He–Cd laser as the excitation source. The commercial scanning tunneling microscope (STM/TEM) holder is used inside the 200 kV TEM (JEM-2010F) to carry out the electrical measurements with a two-terminal configuration. ZnO-Ts

* Corresponding author. Fax: +86 10 62771160.
E-mail address: jzhu@mail.tsinghua.edu.cn (J. Zhu).

0254-0584/$ – see front matter © 2009 Elsevier B.V. All rights reserved.
doi:10.1016/j.matchemphys.2009.11.015

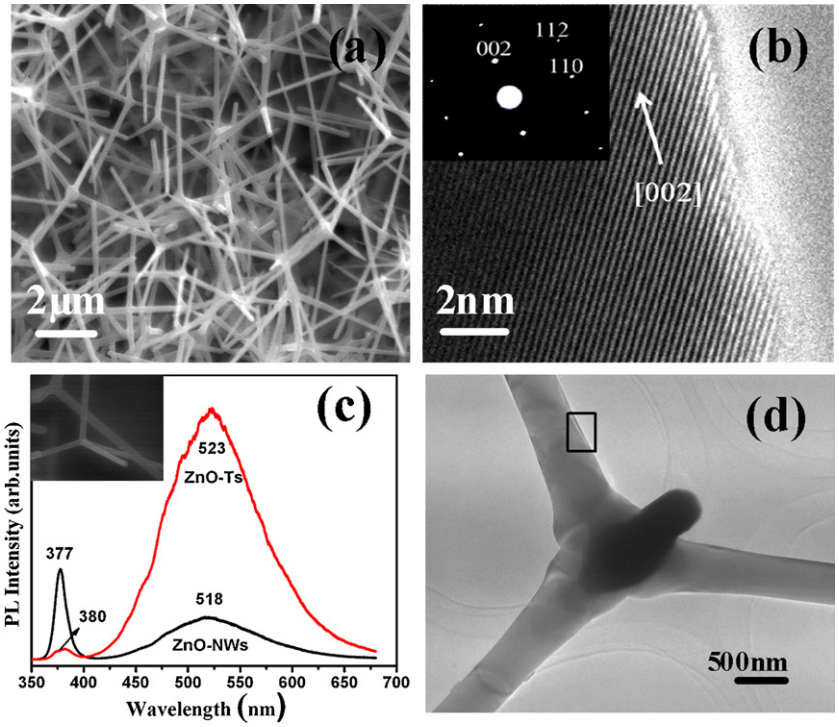

Fig. 1. (a) SEM images of the ZnO-T deposited on the silicon substrate. (b) Bright field HRTEM of ZnO-T taken from the leg (rectangle point) shown in (d); corresponding SAED (see inset). (c) The room temperature PL spectra of ZnO NWs and ZnO-T nanocrystals by using the 325 nm line of a He–Cd laser as the excitation source; SEM image of single ZnO-T (inset). (d) TEM image of individual ZnO-T.

are adhered to a 250-μm diameter Au-electrode. A tungsten (W) tip is piezotube-driven to touch the free end of a protruding ZnO-T on the electrode. The tip can be moved in three dimensions in steps as fine as 0.1 nm. The electron beam is normal to the plane of the electrodes. The vacuum level in the TEM column is $\sim 10^{-5}$ Pa. In order to achieve a good physical contact at the two (arms) ends of the ZnO-T, various approaches are used to minimize the influence of contact resistance R_c. For instance by applying a large bias voltage between the W tip and the Au-electrode to remove the oxide layer on the W tip. Because of the high resistance at the two contacts points of the ZnO-T ends, a locally high temperature by the joule heating could weld the ZnO-T onto its two electrodes, so a perfect electrical contact are realized.

3. Result and discussion

Fig. 1 (a) shows a SEM image of ZnO-T clusters deposited on Si substrate. Each arm is well faceted with a hexagonal cross section and is uniform in length in the range of ~3–15 μm and diameter in the range ~50–300 nm. The angular separation between two hexagonal nanorods is 120°. The morphology and further structure characterizations were also investigated by TEM and HRTEM. Fig. 1(b) shows the HRTEM image of the individual isolated ZnO-T from the point (rectangle) shown in Fig. 1(d) and reveals the single-crystalline nature grown along [0 0 2] preferred direction. The inset shows the corresponding selected area electron diffraction (SAED) pattern, which is consistent with wurtzite structure of ZnO. Fig. 1(d) displays the clearer TEM image of isolated ZnO-T.

Fig. 1(c) shows the room temperature PL spectra of the randomly oriented ZnO-Ts and ZnO nanowires (NWs) prepared under the same experimental conditions for comparison. In the figure, the PL spectra of both ZnO NWs and ZnO-Ts consisted of two parts: one narrow peak in the ultraviolet (UV) region and another broad emission band in visible light (VL) region. In the UV region, the emission peak of ZnO NWs is at about 377 nm and the emission peak of ZnO-Ts is at about 380 nm, which is generally originated from the near-band-edge (NBE) exciton transition in wide bandgap of ZnO, namely the recombination of free excitons through collision process [15]. In VL region, both NWs and ZnO-Ts exhibit broad green luminescence band in the range of 400–680 nm, which is usually related to the defects (such as oxygen vacancy, Zn interstitial) in ZnO structure, in which the emission results from the radiative recombination of photo-generated hole with an electron occupying the defect or oxygen vacancy [16]. By comparison, it can be found that the luminescence band of ZnO-Ts is wider than that of ZnO nanowires, illustrating the increase of defects in ZnO-Ts nanocrystals as reported [17,18]. Also with the comparison of the ratio of UV and VL, the intensity of UV emission peak decreases apparently in ZnO-Ts. The decreases of the UV emission intensity and I_{UV}/I_{VL} in ZnO-T sample are due to the weak exciton Coulomb interaction effect. The shift in peak position of ZnO-T compared to that of NWs can be explained due to the increase of defects. When ZnO-T sample was excited with a He–Cd laser at 325 nm, excitons got up higher energy levels at the bottom of conduction band. Radiative recombination of these excitons leads to a red shift of 3 nm in emission peak of ZnO-Ts spectrum. It has been also seen that the PL emission in ZnO-T does not fall to zero between the UV and broad emission peaks, which indicates the presence of an additional transition in the range 400–450 nm. Emission in the blue spectral range for ZnO has been reported in the literature [19–22]. Possible candidate for transitions in this spectral range are zinc vacancy (405 nm), zinc interstitial (427 nm), and lattice defects related to oxygen and zinc vacancies (420 nm). The peak at 420 nm is also attributed to oxygen interstitial, however, based on theoretical predictions and other experimental results; it is more likely that oxygen interstitial is responsible for yellow emission [23,24]. Up to now, many researchers have demonstrated that the defects play very import role for the tuning of the electrical property of materials [25].

The electrical measurements have been carried out under in situ TEM. Fig. 2(a) shows the measurements of *I–V* curves after establishing a contact between W tip-ZnO-T legs (A and B) and Au-electrode inside TEM. The curve "a" shows the non-Ohmic contacts behavior without the electron beam irradiation and has low forward current (I_f) 11×10^{-9} A, which is due to high resistance and

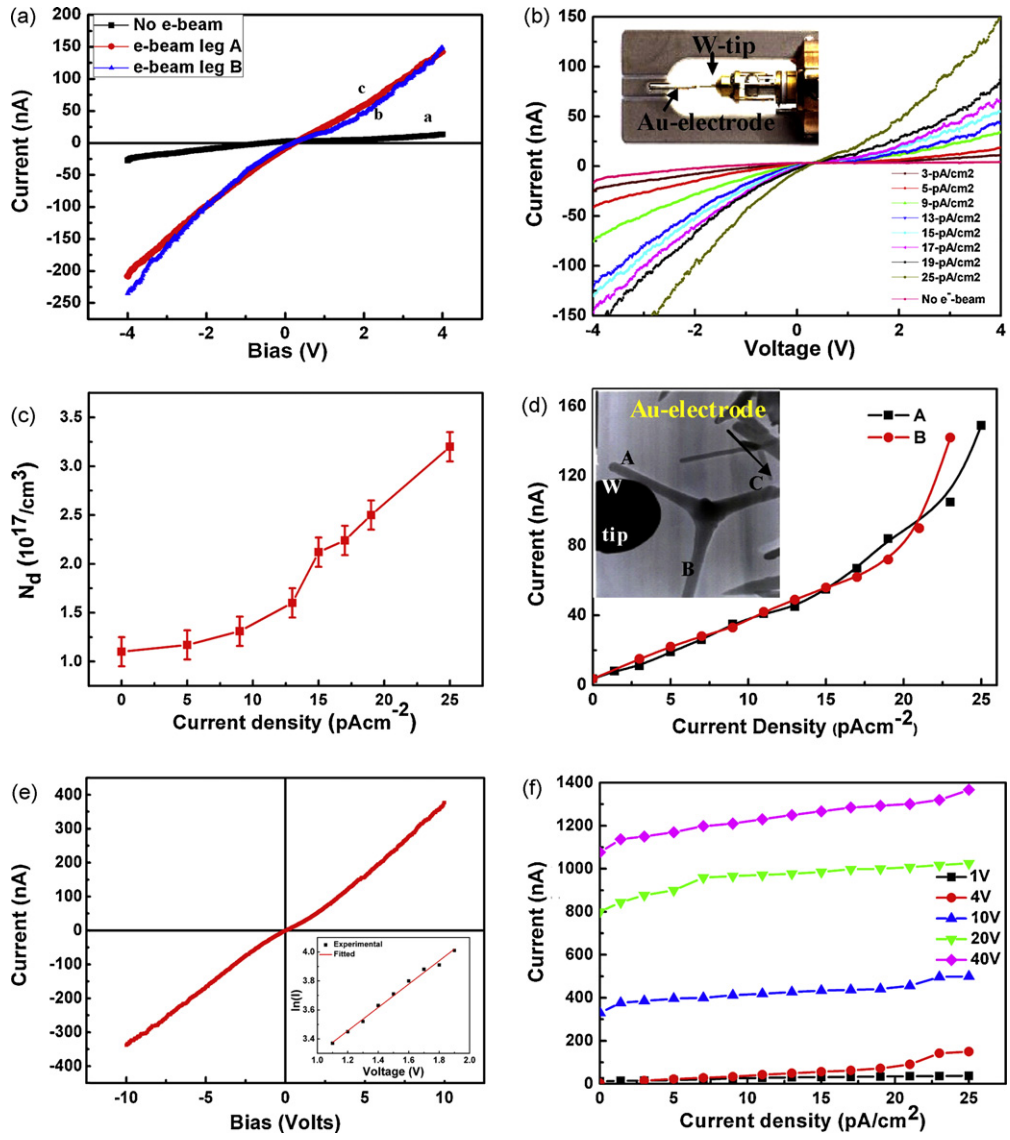

Fig. 2. (a) *I*–V curves of ZnO-T with and without the influence of electron irradiation. (b) *I*–V characteristics of ZnO-T with successive increase in electron density; schematic diagram of TEM-STM holder (inset). (c) Plot of carrier concentration vs electron current density. (d) Current response of legs A and B at different electron current density; inset: TEM image of ZnO-T showing contact between W tip-ZnO-T leg A and Au-electrode for the *I*–V response measurement. (e) High bias *I*–V characteristics of ZnO-T under electron beam; inset (bottom right): experimental and fitted ln(*I*) vs voltage plot at low bias region corresponding to the curve c shown in (a). (f) Electron current density vs current response at voltages 1, 4, 10, 20 and 40 V, respectively.

low carrier density in the structure. The measured results of curves "b" and "c" from the leg A and leg B of shown ZnO-T exhibit asymmetric Schottky behavior under electron beam irradiation. The measurements show a significant increase in the forward current ($I_f = 148 \times 10^{-9}$ A), which clearly demonstrates that the Schottky contacts are formed at the ends of the ZnO-T, under electron beam irradiation.

Fig. 2(b) depicts a series of consecutively recorded *I*–*V* curves corresponding to the successive increase in electron density (from 3 pA cm^{-2} to 25 pA cm^{-2}). All the examined curves have asymmetric Schottky behavior and exhibit a significant enhancement in the current, which is the signature of decrease in the barrier width of interfaces. The increase in the electron density illustrates the increase in the flux of electrons, which derives the excitation of the metal electrode electrons to higher energy states and enhances the tunneling across the metal–semiconductor Schottky barrier. The observed defect states in the prepared ZnO-Ts such as O_i (oxygen interstitial), V_O (oxygen vacancy), Zn_i (zinc interstitial) and V_{Zn} (zinc vacancy) inside the bandgap might assist the tunneling mechanism in the current transport properties under the electron beam irradiation. The inset of Fig. 2(b) is the schematic setup of commercial STM/TEM holder. Fig. 2(c) shows the plot of electron density vs carriers concentration and implies that the interaction of high-energy electrons with ZnO-T induces the formation of electron–hole pairs (e^-/h^+), which may increase the carriers density for electron transport. As the carrier concentration increases, the potential associated with these carriers reduced the width of depletion region at the interface and increased the current. The response of current from the two legs of tetrapod under different electron densities is shown in Fig. 2(d). It is observed that the current shows linear behavior in the range of 3–15 pA cm^{-2}, while beyond this range, an exponential increasing trend is seen, which may be due to the increase in the tunneling probability. Fig. 2d (inset) also shows the label ZnO-T TEM image under in situ measurement and clearly shows the contacts of leg A between W tip and Au-electrode.

Fig. 2(e) shows the *I*–*V* curve taken at the high bias voltage and displays almost linear relation. This linear behavior demon-

strates that at high bias voltage Schottky contacts turn to Ohmic contacts due to the electron–matter interaction at the interfaces. At high bias voltage, the overall resistance of the ZnO-T can be calculated using the relation $R_{ZnO\text{-}T} = dV/dI$ and was found to be 33.48 MΩ. Fig. 2(f) shows the electron density vs current response at different voltages. It has been found that the current response within the same current density range but with different applied voltages shows increasing trend with high voltage. In order to retrieve quantitatively the other intrinsic parameters of the ZnO-T, metal–semiconductor–metal (MSM) model has been applied. Based on the MSM model, the current under the lower bias is expressed as [26].

$$\ln I = \ln(SJ) + V\left(\frac{q}{K_B T} - \frac{1}{E_0}\right) + \ln J_s$$

where J is the current density through the Schottky barrier, S is the contact area associated with the barrier, E_0 is the parameter that depends on the carrier's density, and J_s is the slowly varying function of applied biasing. The logarithmic plot of the current I as a function of the bias voltage as shown in Fig. 2e (inset) gives approximately straight line under the low bias regime of the curve c (in Fig. 2a) and its slope ($k = q/K_B T - 1/E_0$) is used to extract the parameters. Using this technique, the carrier concentrations are calculated with and without electron beam irradiation and their corresponding values are $n = 3.2 \times 10^{17}\ cm^{-3}$ and $n = 1.1 \times 10^{17}\ cm^{-3}$, respectively. These calculated values are well in agreement with the standard ZnO material.

4. Conclusions

In conclusion, in situ measurements have shown that ZnO-T is very sensitive to electron irradiation with a lowest limit of electron density ~3 pA cm^{-2}. I–V characteristics have demonstrated that the Schottky contacts are formed at the both ends, which turn to Ohmic at high bias voltage due to electron–matter interaction. The results have also depicted that the increase in the electron density leads to an increase in carrier concentration. Furthermore, it is found that the defects also play significant role to assist the tunneling of electrons in the transport mechanism of ZnO-T. These results suggest that ZnO-T can be useful for the fabrication of optoelectronics devices (such as photo and radiation detectors).

Acknowledgment

This work is financially supported by the National 973 Project of China and Chinese National Nature Science Foundation. The authors also thanks the Higher Education Commission (HEC) Pakistan for the financial support to Mashkoor Ahmad.

References

[1] M.H. Huang, S. Mao, H. Feick, H. Yan, Y. Wu, K. Kind, E. Weber, R. Russo, P. Yang, Science 292 (2001) 1897.
[2] Z.W. Pan, Z.R. Dai, Z.L. Wang, Science 291 (2001) 1974.
[3] M.C. Newton, F. Steven, A. Paul, J. Phys. Conf. Ser. 26 (2006) 251.
[4] L. Manna, E.C. Scher, A.P. Alivisatos, J. Am. Chem. Soc. 122 (2000) 12700.
[5] J.F. Gong, S.G. Yang, H.B. Huang, J.H. Duan, H.W. Liu, X.N. Zhao, et al., Small 2 (2006) 732.
[6] F.Z. Wang, Z.Z. Ye, D.W. Ma, L.P. Zhu, F. Zhuge, Mater. Lett. 59 (2005) 560.
[7] S.S. Fan, M.G. Chapline, N.R. Franklin, T.W. Tombler, A.M. Cassel, H.J. Dai, Science 283 (1999) 512.
[8] D.C. Look, C. Coskun, B. Claafan, G.C. Forlow, Physica B 32 (2003) 340.
[9] D.C. Look, D.C. Reynolds, J.W. Hemsky, R.L. Jones, J.R. Sizelove, Appl. Phys. Lett. 75 (1999) 811.
[10] C. Coskun, D.C. Look, G.C. Forlow, J.R. Sizelove, Semicond. Sci. Technol. 19 (2004) 752.
[11] K. Svensson, Y. Jompol, H. Olin, E. Olsson, Rev. Sci. Instrum. 74 (2003) 4945.
[12] M.C. Newton, F. Steven, A. Paul, Warburton, Appl. Phys. Lett. 89 (2006) 072104.
[13] M.C. Newton, et al., 6th IEEE Conference on Nanotechnology, vol. 2, Cincinnati, OH, 2006, p. 453.
[14] Y.W. Heo, L.C. Tien, Y. Kwon, D.P. Norton, S.J. Pearton, Appl. Phys. Lett. 85 (2004) 2274.
[15] Y.C. Kong, D.P. Yu, B. Zhang, W. Fang, S.Q. Feng, Appl. Phys. Lett. 78 (2001) 407.
[16] K. Vanheusden, W.L. Warren, C.H. Seager, D.K. Tallant, J.A. Voigt, B.E. Gnade, J. Appl. Phys. 79 (1996) 7983.
[17] Y. Dai, Y. Zhang, Q.K. Li, C.W. Nan, Chem. Phys. Lett. 358 (2002) 83.
[18] A.B. Djurisic, W.C.H. Choy, V.A.L. Roy, Y.H. Leung, C.Y. Kwong, K.W. Cheah, T.K. Gundu Rao, W.K. Chan, H.F. Lui, C. Surya, Adv. Funct. Mater. 14 (2004) 856.
[19] B.J. Jin, S. Im, S.Y. Lee, Thin Solid Films 366 (2000) 107.
[20] X.L. Wu, G.G. Siu, C.L. Fu, H.C. Ong, Appl. Phys. Lett. 78 (2001) 2285.
[21] S. Mahamuni, K. Borgohain, B.S. Bendre, V.J. Leppert, S.H. Risbud, J. Appl. Phys. 85 (1999) 2861.
[22] J.Q. Hu, X.L. Ma, Z.Y. Xie, N.B. Wong, C.S. Lee, S.T. Lee, Chem. Phys. Lett. 344 (2001) 97.
[23] B. Lin, Z. Fu, Y. Jia, Appl. Phys. Lett. 79 (2001) 943.
[24] M. Lu, A.H. Kitai, P. Mascher, J. Lumin. 54 (1992) 35.
[25] M.W. Ahn, K.S. Park, J.H. Heo, J.G. Park, D.W. Kim, K.J.I. Choi, J.H. Lee, S.H. Hong, Appl. Phys. Lett. 93 (2008) 263103.
[26] X.D. Bai, D. Golberg, Y. Bando, C.Y. Zhi, C.C. Tang, M.K. Kurashima, Nano Lett. 7 (2007) 632.